JMES The International Journal of Mechanical Engineering and Sciences
https://iptek.its.ac.id/index.php/jmes
e-ISSN 2580-7471

Experimental Study on the Flexural Performance of Sustainable Composites Utilizing Processed Solar Panel Waste

Ikko Yuswanda[1], Yi Chieh Wu[2], Betti Ses Eka Polonia[1,4], Dinny Harnany[1,3], Muhammad Akhsin Muflikhun[1,5*]

[1]Department of Mechanical and Industrial Engineering, Faculty of Engineering, Universitas Gadjah Mada, Yogyakarta, 55281, Indonesia
[2]National Chengchi University, Taipei City, Taiwan 116
[3]Department of Mechanical Engineering, ITS, Sukolilo Surabaya 60111, Indonesia
[4]Politeknik Negeri Ketapang, Ketapang, Kalimantan Barat 78813, Indonesia
[5]Center for Energy Studies, Universitas Gadjah Mada, Yogyakarta, Indonesia

Received: 27 February 2026, Revised: 05 March 2026, Accepted: 10 March 2026

Abstract

The rise in end-of-life photovoltaic (PV) waste necessitates recycling pathways. This study pioneers the utilization of PV waste powder as a filler in Digital Light Processing (DLP) 3D-printed resin composites. Three variations, SN 2 (coarse), SN 4 (medium), and SN 6 (fine) were incorporated into a photopolymer matrix and characterized using SEM-EDX, FTIR, and flexural testing. Results reveal a 73% increase in flexural strength, peaking at 33.11 MPa for the SN 2 composite compared to 19.13 MPa for the neat resin. SEM analysis indicates that the angular silicon-based particles in SN 2 effectively diverted crack propagation and facilitated micro-mechanical interlocking, transforming the fracture mechanism from brittle failure to a toughened, energy-absorbing mode. EDX analysis confirmed high silicon purity in the reinforcing phase, while FTIR verified that the filler interaction remained purely physical, preserving the resin's chemical stability. The finest SN 6 fraction exhibited reduced performance due to particle agglomeration driven by the highly cohesive nature of the fine powder, which acted as stress concentrators, alongside impurity concentration (Rb/Nb) in the dust. These findings demonstrate that upcycling PV waste into DLP materials offers a sustainable, low-cost solution that significantly enhances mechanical performance without requiring complex chemical modification, provided that the particle size is carefully optimized to balance dispersion and interfacial bonding.

Keywords: Flexural Strength, Photovoltaic, Waste, Composite, Digital Light Processing

1. Introduction

The worldwide transition to renewable energy has positioned solar photovoltaics (PV) as a fundamental component of the contemporary power system. The imperative to decarbonize the energy industry has led to an extraordinary increase in the installed capacity of solar modules. Nonetheless, this swift expansion presents a considerable environmental concern: the disposal of end-of-life (EoL) solar modules [1, 2]. Standard silicon-based photovoltaic modules generally have a lifespan of about 25 to 30 years, after which they are retired [3]. Forecasts indicate that by 2050, the total waste generated by these modules may attain 78 million tons worldwide [4, 5]. In the absence of effective recycling systems, these modules are often disposed of in landfills, resulting in both the depletion of valuable resources and a considerable environmental hazard.

The environmental issue regarding end-of-life photovoltaic waste is chiefly attributed to the presence of toxic metals in the cell structure [6, 7]. Conventional waste characterization experiments, such as the Toxicity Characteristic Leaching Procedure (TCLP), have shown that heavy metals such as lead (Pb) and cadmium (Cd) can leach into municipal solid waste (MSW) leachate under certain conditions [4]. Although actual landfill circumstances may yield reduced leaching rates compared to conventional laboratory assessments, the enduring threat of soil and groundwater pollution demands a transition from landfilling to circular management [4]. Life cycle assessments (LCA) substantiate the imperative for this transition; for example, recycling silicon-based photovoltaic modules in India has demonstrated a reduction in global warming potential (GWP) by 48% to 49% relative to conventional disposal methods such as landfilling or incineration [3].

While effective separation techniques are critical for managing end-of-life photovoltaic (PV) modules, the subsequent reutilization of these recovered materials offers

*Corresponding author. Email: akhsin.muflikhun@ugm.ac.id

an equally significant opportunity for sustainable engineering [8, 9]. Rather than simply diverting waste from landfills, recent research suggests that recovered components, particularly silicon and glass, can be valorized as functional reinforcements in polymer matrices [6, 10]. For instance, solar-grade silicon particles retrieved from wafer production waste have been successfully employed as fillers in epoxy-glass fiber composites, demonstrating a linear improvement in both flexural strength and hardness. Similarly, silica-based glass recovered from waste electrical and electronic equipment (WEEE), including PV infrastructure, is being explored to enhance the thermal and mechanical performance of thermoplastic filaments [11]. These applications not only mitigate the environmental footprint associated with raw material extraction but also provide a cost-effective strategy for producing high-performance structural materials. Building on these findings, this study experimentally investigates the flexural performance of sustainable composites fabricated using processed solar panel waste, aiming to establish a viable pathway for closing the loop in the photovoltaic lifecycle [6, 7].

A substantial byproduct of the recycling and manufacturing process is waste containing silicon and silica [12]. A significant quantity of solar-grade silicon is lost as kerf particles during the slicing of silicon ingots [10]. Moreover, the pulverization of module glass generates a substantial quantity of silica debris. Recent advancements in particle separation, including innovative sieving aids and upstream pyrolysis, have enhanced the recovery rates of precious chip-like photovoltaic cell particles from waste mixes [8]. Although the recovery of high-value silver is frequently the economic focus, repurposing the predominant silicon and silica waste as useful fillers in composite materials offers a significant open-loop recycling prospect [12].

The addition of waste-derived fillers into polymer matrices effectively improves mechanical performance and decreases material expenses. The use of economical biomass- or industrial waste-derived functional ceramic fillers, such as biogenic silicon nitride (Si_3N_4) or silicon carbide (SiC), has demonstrated enhancements in the mechanical and thermal properties of epoxy composites [13–15]. The incorporation of reclaimed silicon wafer kerf particles as a filler in epoxy-glass fiber polymer composites has produced encouraging outcomes. The incorporation of silicon particles, especially those smaller than 10 μm, resulted in a linear enhancement of both hardness and flexural strength [10]. The inclusion of these stiff particles in the matrix enhances load distribution and inhibits rapid crack formation under bending stress.

Flexural performance is an essential criterion for sustainable composites, as it dictates their appropriateness for structural or semi-structural applications in the construction and automotive sectors. The reinforcing efficacy of silica- and silicon-based fillers is mostly contingent upon their dispersion and interfacial adhesion with the matrix. Research on silica-reinforced polylactic acid (PLA) for 3D printing applications indicates that although silica can improve heat stability and rigidity, the filler concentration must be meticulously calibrated to avoid embrittlement [11]. Hybrid systems that integrate natural fibers with waste-derived SiC particles provide a synergistic effect, where the fibers contribute ductility and the ceramic fillers confer essential stiffness to improve flexural limits [14].

Considering the expanding literature on material recovery from photovoltaic waste, a gap persists in comprehending the complete mechanical potential of "processed" solar panel waste. While silicon and silica are extracted via specific delamination and etching techniques, within a sustainable composite framework [5, 16]. Most research concentrates on either recycling technologies or the characteristics of virgin ceramic fillers. This study seeks to address this gap by conducting an experimental analysis of the flexural performance of composites made from processed solar panel waste. This research aims to validate a high-value application for PV waste by analyzing the effects of filler loading [15], particle morphology, and processing history on flexural strength and stress-strain behavior, thereby facilitating the transition to a genuine circular solar economy.

2. Experimental method

2.1. Materials

The polymer matrix employed in this study was Anycubic Standard Resin V2 Clear, chosen for its consistent mechanical performance and compatibility with the DLP printing process. The reinforcing agents were derived from processed solar panel waste provided by PT. Wijaya Karya Industri Energi (Persero) Tbk, comprising recovered silicon and silica particles as rigid fillers. Furthermore, recycled PV material obtained from retired solar backsheets was utilized to evaluate its potential as a sustainable structural reinforcement.

2.2. Specimen manufacturing

PV waste plates were processed with the Orion Herb & Spice Grinder MG-300B to produce a fine PV powder. The powder was subsequently sieved using test sieve meshes of 200/75 μm, 400/38 μm, and 600/30 μm to attain a homogeneous particle distribution as specified. PV powder that passes sieve number 200 but does not pass sieve number 400 is called SN 2, sieve number 400 but does not pass sieve number 600 is called SN 4, and that which passes sieve number 600 is called SN 6. The composition of each specimen is shown in Table 1. The filler loading was maintained at a constant 0.1 wt% for all variations to ensure optimal UV light penetration during the DLP process, as higher loadings of opaque silicon-based fillers can induce significant light scattering, leading to incomplete photopolymerization and printing failure. Furthermore, adopting a minimal concentration allows for a fundamental evaluation of the filler's reinforcing efficiency, as it is crucial to observe the initial reinforcement thresh-

Table 1. Composition of resin and PV powder.

Specimen ID	Resin (%wt)	PV (%wt)	Sieve Number	Number of specimen
Resin	100	0	–	3
SN 2	99.9	0.1	200–400	3
SN 4	99.9	0.1	400–600	3
SN 6	99.9	0.1	600	3

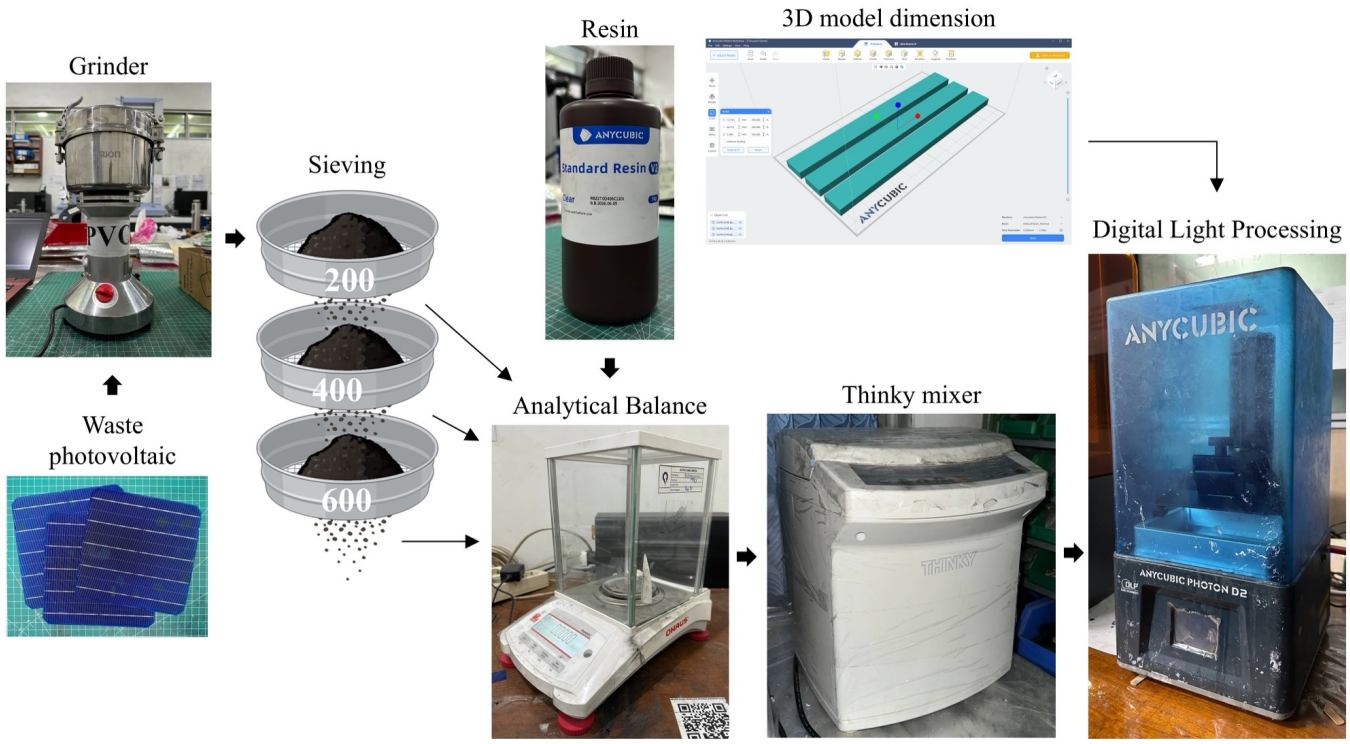

Figure 1. Specimen manufacturing.

old before the composite system reaches saturation. It is also noted that a larger quantity of particles does not necessarily yield a significant positive impact; instead, excessive loading may lead to particle agglomeration, which frequently results in a reduction of structural integrity rather than further enhancement. Following the screening operation, the PV powder was meticulously weighed utilizing an Ohaus Pioneer PX224 Analytical Balance to guarantee that the mixture composition adhered to the required weight percentage in the study design.

The subsequent phase involves the incorporation of PV powder into the resin, which is then agitated using a Planetary Thinky Mixer ARE-310. This procedure integrates concurrent mixing (3 minutes at 2000 rpm) and defoaming (2 minutes at 2200 rpm) to yield a uniform, air-bubble-free blend. This uniform combination is subsequently utilized as a specimen printing material in an Anycubic Photon D2 DLP printer, with printing parameters calibrated to guarantee optimal dimensional accuracy and mechanical integrity. The aforementioned production procedure is crucial for ensuring high specimen quality.

The printed specimens were subsequently examined for physical defects, such as fractures or voids. To ensure dimensional accuracy, each specimen was measured using a digital caliper in accordance with ASTM D790 standards, targeting nominal dimensions of 127 mm in length, 12.7 mm in width, and 5 mm in thickness. Any specimen deviating significantly from these specifications was reprinted using the DLP 3D printing process.

The average thickness measured for each variation group was utilized to determine the support span length, which was set at a span-to-depth ratio of 16:1 (approximately 80 mm). To ensure data reliability, three replicates were tested for each variation, and the average value was calculated. The results were then compared with the baseline performance of the 100% neat resin matrix. If a specimen exhibited a premature failure significantly below the baseline, indicating a manufacturing defect rather

than material behavior, it was reproduced. The complete specimen preparation workflow is illustrated in Figure 1. Flexural testing was performed to evaluate the material's capacity to endure bending stresses and to ascertain its elastic limit and fracture strength [17].

2.3. Specimens Characterization

2.3.1. Morphological using Dino-Lite and SEM

Morphological analysis was conducted to evaluate the structural integrity and failure mechanisms of the sustainable composites. Initially, a 5 MP Dino-Lite Edge digital microscope (AM7515 - Taipei, Taiwan) was employed for the macroscopic inspection of the raw PV powder. This preliminary observation served to identify the general particle shape and size distribution of the fillers prior to fabrication.

Following this, Scanning Electron Microscopy (SEM - Thermo Scientific PHENOM-PROX, US) was utilized to perform a high-resolution microstructural examination of the fractured composite surfaces. Prior to imaging, the non-conductive specimens were sputter-coated with a thin layer of gold to induce surface conductivity and prevent charging artifacts. The primary objective of the SEM analysis was to assess the interfacial adhesion between the processed solar panel waste fillers, specifically recovered silicon and silica the clear resin matrix. SEM imaging facilitated a qualitative evaluation of filler dispersion and the detection of micro-agglomerations, which play a critical role in determining the material's flexural strength. Furthermore, the surface texture observed via SEM provided insights into the mechanical interlocking mechanism; coarser fracture surfaces typically indicate enhanced energy absorption and load-bearing capacity.

2.3.2. FTIR

Fourier Transform Infrared Spectroscopy (FTIR - SHIMADZU IRXross, JAPAN) is employed to examine the chemical composition and molecular interactions of the sustainable composite. FTIR determines the functional groups in the conventional resin, recycled PV, and processed solar panel waste by measuring their infrared absorption spectra [18]. The principal role of FTIR is to identify whether new chemical bonds are formed or if the interaction remains purely physical upon the incorporation of reclaimed silicon and silica fillers. It assists in confirming whether the recycling process has resulted in organic residues and evaluates the interfacial compatibility between the matrix and filler. Comprehending these molecular attributes is essential, as the nature of the interface whether it is governed by chemical bonding or physical mechanisms like mechanical interlocking is directly linked to the composite's capacity to transmit stress efficiently, hence influencing its flexural performance.

2.4. Density and Void Fraction Analysis

Experimental density (ρ_{exp}) testing was conducted in accordance with the ASTM D792 standard using Archimedes' principle. Test specimens were specifically printed with dimensions of $20 \times 20 \times 3$ mm. Mass measurements were performed using a high-precision analytical balance (Ohaus Pioneer PX224). Each measurement was conducted in triplicate to ensure data accuracy and to obtain the mean values and standard deviations. The samples were first weighed in air to obtain their dry mass (W_a), and subsequently weighed while fully immersed in demineralized water at room temperature $(25°\mathrm{C})$ to determine their wet mass (W_w). The experimental density was then calculated based on the mass difference relative to the density of the immersion liquid.

Furthermore, void fraction analysis was conducted to evaluate the quality of the 3D printing process and to quantify the percentage of macroscopic air entrapped within the composite matrix. The void fraction (v_v) was calculated by comparing the theoretical density (ρ_{th}) with the experimental density (ρ_{exp}) using the following Equation 1:

$$v_v(\%) = \frac{\rho_{th} - \rho_{exp}}{\rho_{th}} \times 100 \tag{1}$$

The theoretical density of the composite (ρ_{th}) was determined using the Rule of Mixtures based on the weight fractions of its constituents, as expressed in Equation 2:

$$\rho_{th} = \frac{100}{\left(\frac{W_f}{\rho_f}\right) + \left(\frac{W_m}{\rho_m}\right)} \tag{2}$$

where W_f and W_m represent the weight fractions (wt%) of the PV reinforcing powder (0.1 wt%) and the resin matrix (99.9 wt%), respectively. Meanwhile, ρ_f and ρ_m denote the theoretical densities of each respective material. Considering that the primary constituent material in solar cell (PV) waste is silicon, the standard literature density for pure silicon, 2.33 $\mathrm{g/cm^3}$, was used to represent the particle density value (ρ_f).

2.5. Flexural Test

Flexural strength testing was employed as the principal mechanical characterization technique to assess the load-bearing capability and structural integrity of the sustainable composites [16, 17]. The testing was conducted using a Shimadzu Autograph AGS-X 10 kN Universal Testing Machine (Shimadzu Corp., Kyoto, Japan), as illustrated in Figure 3. Performed using a three-point bending configuration, this test evaluates the material's capacity to withstand deformation under transverse loading. The flexural stress (σ_f) and flexural strain (ε_f) were determined using the following standard equations:

$$\sigma_f = \frac{3FL}{2bd^2} \tag{3}$$

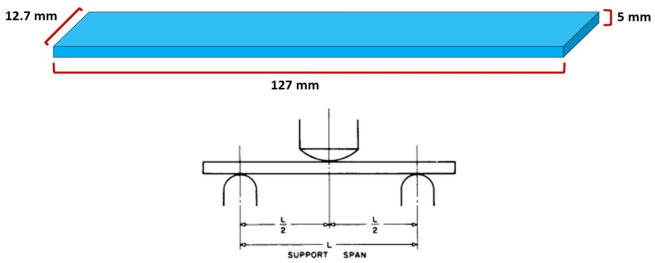

Figure 2. Specimen dimension and schematic flexural test illustration based on ASTM D790 [17].

$$\varepsilon_f = \frac{6Dd}{L^2} \tag{4}$$

where σ_f is the flexural stress (MPa), ε_f is the flexural strain (mm/mm), F is the applied load (N), L is the support span length (mm), b is the width of the specimen (mm), d is the thickness of the specimen (mm), and D is the maximum deflection at the center of the beam (mm). The ultimate flexural strength is defined as the maximum stress sustained by the specimen before failure. This assessment is critical for determining the impact of integrating processed solar panel waste, specifically recovered silicon and silica on the composite's stiffness and ultimate strength.

This study measures the reinforcing efficacy of PV waste-derived fillers within the resin matrix by calculating stress, peak stress, and strain. Ultimately, the findings confirm the viability of utilizing photovoltaic waste in structural applications where resistance to bending is crucial. The specimen dimensions are presented in Figure 2. The experimental setup for the flexural strength test is illustrated in Figure 3.

3. Result and Discussion

3.1. Surface Morphology

Morphological characterization of the raw photovoltaic waste filler, processed through three distinct sieving stages: Mesh 200 (SN 2), Mesh 400 (SN 4), and Mesh 600 (SN 6) is presented in Figure **??**. Macroscopic inspection via Dino-Lite (414x magnification, left column) reveals distinct textural differences in the bulk powder. The SN 2 sample exhibits a coarse, granular morphology with clearly separable, sand-like particles (Figure **??**C). In contrast, as the mesh size increases, the SN 4 and SN 6 powders display a progressively smoother and more cohesive appearance (Figure **??**B and A), indicating a higher packing density and a reduction in inter-particle voids within the bulk powder pile.

To quantify this particle refinement, microstructural analysis was conducted using SEM (1000x magnification, right column). All samples display angular, irregular crystalline structures typical of mechanically milled photovoltaic precursors. The SN 2 variation (retained by the 75 μm sieve) contains the coarsest particles, with primary grains measuring between approximately 87 μm and 103

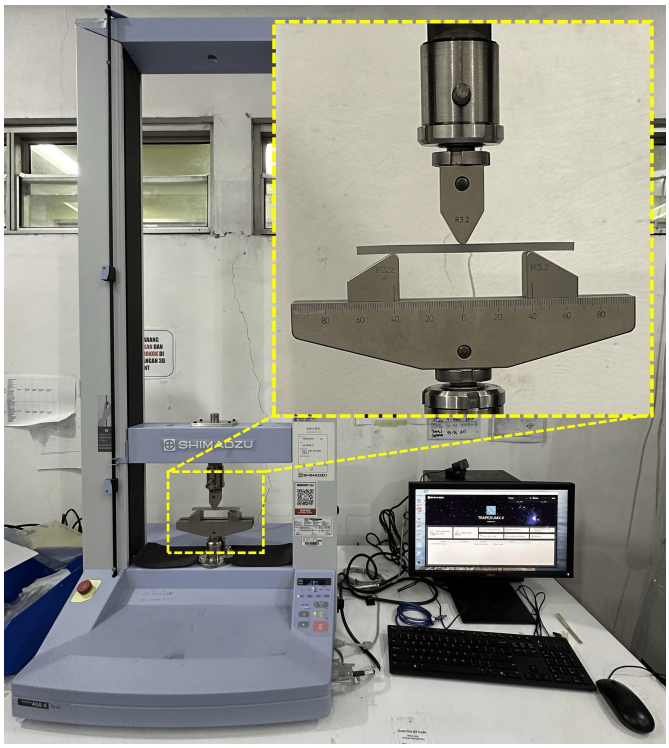

Figure 3. Flexural test using Shimadzu UTM.

μm. The distribution is relatively uniform with minimal fine dust. A marked reduction in grain size is observed in the SN 4 sample (passing the 38 μm sieve), with particles ranging from 39 μm to 52 μm, though a higher degree of heterogeneity is evident as smaller fragments fill the interstitial spaces. Finally, the SN 6 sample (passing the 30 μm sieve) yields the most refined powder, with particle sizes predominantly in the 23 μm to 37 μm range. This systematic reduction in particle size confirms the efficacy of the sieving process in producing three distinct filler grades. Despite the variation in dimensions, the angular geometry remains consistent across all samples, preserving the fundamental physical characteristics of the processed photovoltaic waste prior to composite fabrication. However, the cohesive nature observed in the macroscopic images also suggests a higher tendency for agglomeration, aligning with saturation challenges described by Lakshmaiya et al. [14] and Stratiotou Efstratiadis et al. [11] in similar particulate-reinforced systems.

Complementing the particle size analysis in Figure **??**, the chemical composition of the sieved powders was investigated via SEM-EDX, as presented in Figure 4. The SEM micrographs focus on individual particle surfaces, with SN 2 viewed at $2500\times$ magnification (Figure 4C), while the finer SN 4 and SN 6 fractions are examined at $5000\times$ magnification (Figure 4B and 4A). Consistent with previous morphological observations, the particles retain their angular, irregular crystalline geometry across all variations.

The Energy Dispersive X-ray (EDX) spectra reveal a distinct shift in elemental composition relative to particle

size. Silicon (Si) remains the dominant matrix element in all samples, confirming the core material identity. The coarse SN 2 fraction (Figure 4C) exhibits the highest purity, with silicon accounting for 97.6% of the atomic concentration (A.C.), accompanied by trace amounts of aluminum. However, a significant compositional change occurs in the finer fractions. In SN 4 (Figure 4B) and SN 6 (Figure 4A), the spectra detect the emergence of rubidium (Rb) and niobium (Nb) alongside silicon.Notably, rubidium appears in substantial quantities by weight, recording a Weight Concentration (W.C.) of 17.6% in SN 4 and 17.3% in SN 6, while niobium reaches a W.C. of approximately 4.2% to 5.1%. It must be noted that this EDX analysis was conducted using a point-scan method, which captures highly localized surface measurements. Therefore, these extraordinary values do not represent the bulk composition of the PV powder. Instead, they indicate that the localized electron beam targeted isolated fragments of impurities. This supports the premise that trace materials likely derived from anti-reflective coatings, dopants, or conductive layers are more brittle and preferentially pulverized into the finer dust fractions during the milling process. From a mechanical perspective, the accumulation of these brittle micro-fragments acts as stress concentrators within the polymer matrix. Rather than reinforcing the resin, these localized impurities disrupt uniform load transfer, which directly contributes to the reduced flexural strength observed in the SN 4 and SN 6 composites compared to the purer SN 2 variant. Despite these variations, the high silicon content (> 90 at%) across all samples validates the material's suitability as a rigid, high-modulus reinforcement.

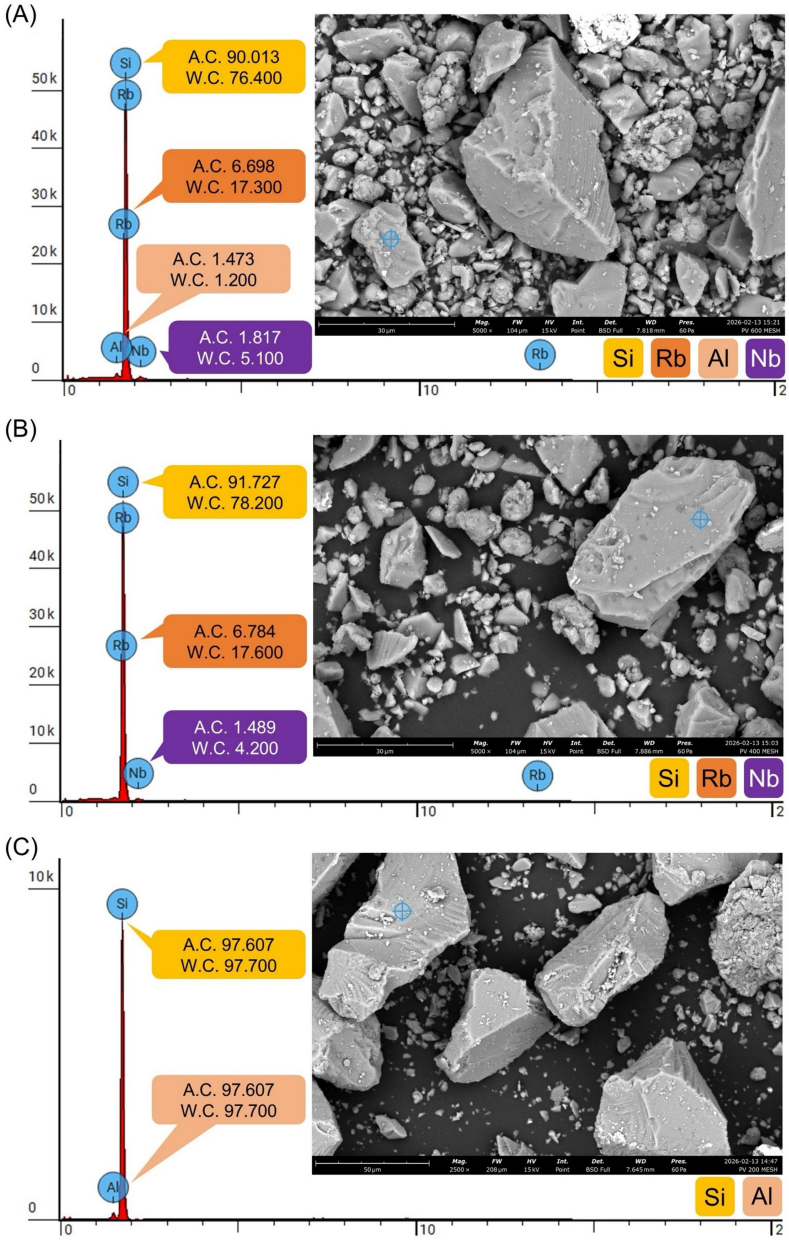

Figure 4. SEM-EDX analysis of photovoltaic powder, (A) SN 6, (B) SN 4, (C) SN 2.

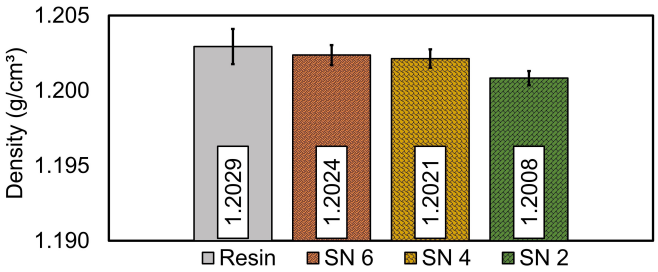

Figure 5. Density with standard deviation of various specimens.

3.2. Density and Void Fraction Analysis

To further evaluate the physical quality of the 3D-printed composites and rule out macroscopic printing defects, experimental density measurements and void fraction analyses were conducted. Using a theoretical density of 2.33 $\mathrm{g/cm^3}$ for the silicon-rich PV filler, the theoretical density of the 0.1 wt% composite was calculated to be 1.2035 $\mathrm{g/cm^3}$. Based on the mean experimental densities of 1.2024 $\pm$ 0.00067, 1.2021 $\pm$ 0.00061, and 1.2008 $\pm$ 0.00047 $\mathrm{g/cm^3}$ for the SN 6, SN 4, and SN 2 composites, respectively compared to the neat resin at 1.2029 $\pm$ 0.00117 $\mathrm{g/cm^3}$, the resulting void fractions are exceptionally low at 0.09%, 0.12%, and 0.22% (Figure 5).

These negligible void fractions ($<$0.25%) indicate optimal curing and consolidation during the DLP printing process, confirming that the incorporation of the PV powder did not lead to significant air entrapment. Interestingly, the SN 6 composite exhibits the highest relative density and the lowest void fraction among the reinforced groups. This is likely due to the ultra-fine particles efficiently filling the interstitial spaces within the polymer network. Because the SN 6 variation concurrently exhibits the lowest flexural strength, this quantitative void analysis conclusively rules out bulk porosity as the mechanism of failure. Instead, it firmly corroborates that the mechanical degradation in the finer variations is entirely driven by the localized micro-agglomeration of brittle trace elements as observed in the SEM and EDX analyses, Figure 7 acting as severe stress concentrators, rather than poor printability or structural voids.

3.3. Flexural Properties

The flexural test results, illustrated through the stress-strain curves shown in Figure 6. The curves demonstrate a significant enhancement in the mechanical strength of the resin upon the incorporation of photovoltaic fillers. The neat resin exhibits the highest ductility but the lowest peak strength, reaching a maximum stress of approximately 20 MPa with a strain at failure exceeding 13%. This profile indicates a relatively flexible and tough material. In materials science, flexibility is evidenced by the high strain at failure (exceeding 13%), which allows the neat resin to undergo significant deformation without breaking. Furthermore, this extended elongation contributes to a larger integrated area under the stress-strain curve. This substantial area signifies the material's ability to absorb considerable energy before ultimate fracture, which is the defining characteristic of mechanical toughness.

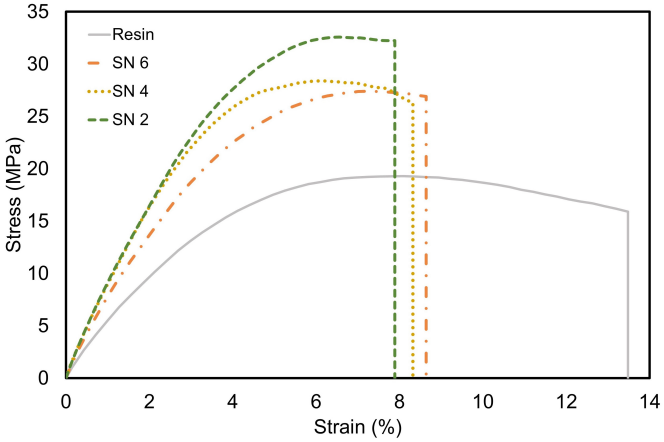

Figure 6. Stress-strain curves of various specimens.

In contrast, the addition of PV fillers in samples SN 2, SN 4, and SN 6 dramatically increases the flexural strength while reducing the material's elongation capacity, marking a transition toward a more rigid and brittle behavior. Sample SN 2 achieves the highest ultimate flexural strength, peaking at roughly 33 MPa, which represents a substantial improvement over the pure resin. However, as the particle size decreases in SN 4 and SN 6, a gradual decline in maximum stress is observed compared to SN 2, though they remain significantly stronger than the neat resin at approximately 27-28 MPa. All filler-loaded composites exhibit a sharply truncated strain, failing between 8% and 9%. This suggests that while the PV powder effectively reinforces the matrix, higher loading levels may introduce particle agglomeration or stress concentrators that slightly limit the peak reinforcement potential.

The ultimate flexural strength results of the photovoltaic composite materials, conducted via three-point bending shown in Figure 8. The graph reveals a significant enhancement in mechanical performance compared to the neat resin. According to the stress-strain data, the neat resin exhibits a ductile profile with a maximum flexural strength of 19.13 $\pm$ 1.83 MPa and a high failure strain of approximately 13.5%. The introduction of PV filler transitions the material behavior from ductile to quasi-brittle, characterized by increased stiffness and reduced elongation at break.

The results demonstrate a clear correlation between the filler type and the ultimate strength of the composite. Sample SN 2, which utilizes a 200-400 mesh filler, achieves the highest flexural strength at 33.11 $\pm$ 1.85 MPa, representing a 73% increase over the base resin. As the filler particle size or distribution changes in samples SN 4 (400-600 mesh) and SN 6 (600 mesh), the flexural strengths reach 28.62 $\pm$ 0.57 MPa and 25.65 $\pm$ 3.59 MPa, respectively. While all reinforced samples outperform the

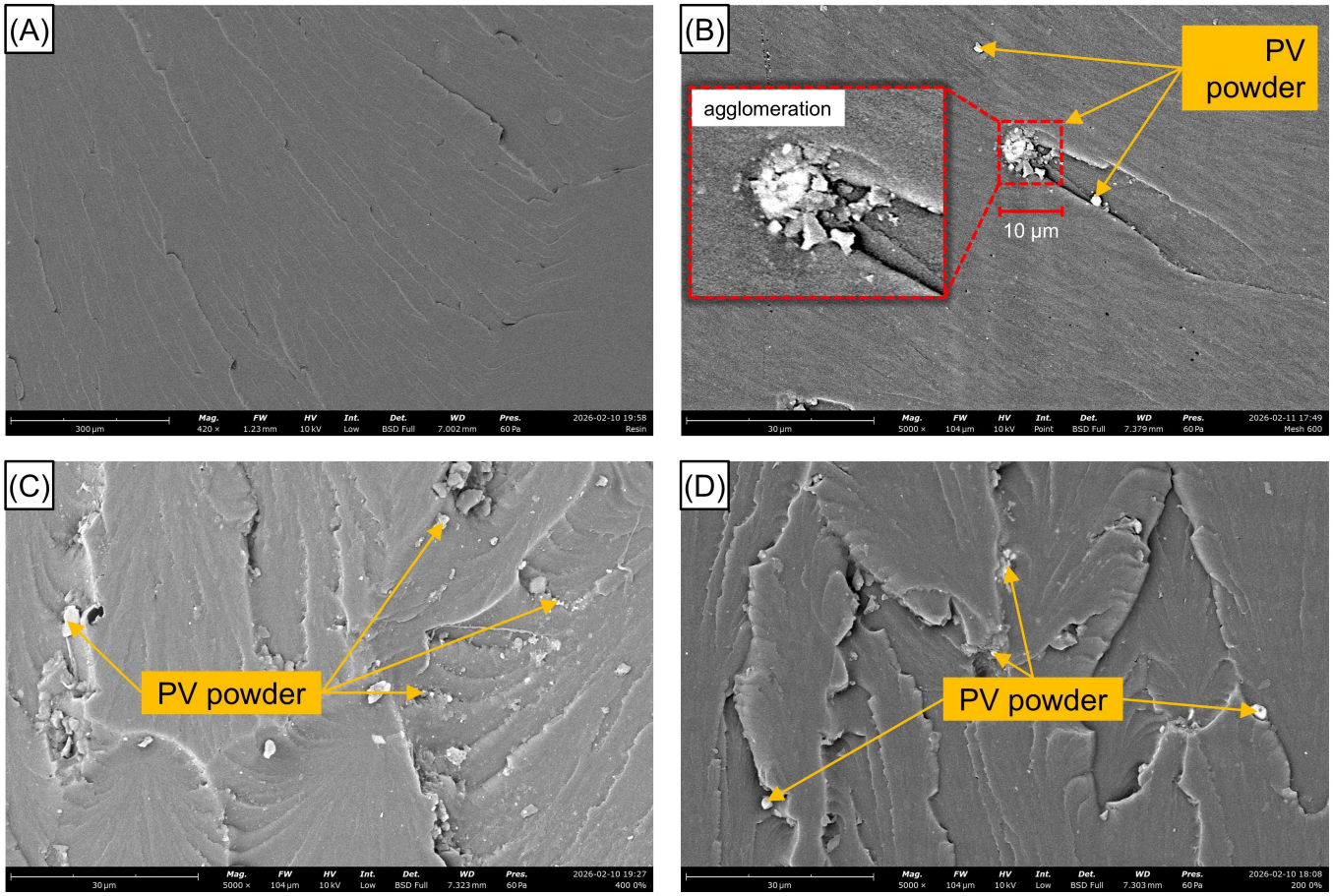

Figure 7. Fracture surface morphology observed by SEM: (A) Resin, (B) SN 6, (C) SN 4 and (D) SN 2.

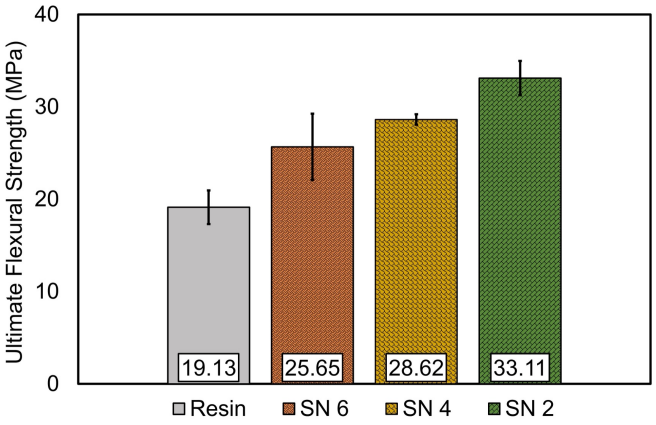

Figure 8. Ultimate Flexural Strength of various specimens.

neat resin, the SN 2 variant provides the most effective load transfer within the matrix. This mechanical reinforcement is further supported by the SEM observations, where the filler particles act as barriers to crack propagation, resulting in the scaly, textured fracture surfaces seen in the loaded composites compared to the smooth river-lines of the pure resin.

The integration of photovoltaic waste powder as a filler markedly improved the mechanical properties of the DLP-printed resin composites, validating the potential of waste-derived reinforcements. The results indicated that the incorporation of PV powder enhanced the flexural strength of the unmodified resin from 19.13 MPa to a maximum of 33.11 MPa with the SN 2 filler (coarsest fraction). This improvement aligns with findings that rigid microfillers, such as silica and silicon, efficiently transfer stress from the polymer matrix, thereby enhancing stiffness and strength [15].

Interestingly, a reduction in strength was observed in the finer filler variations (SN 4 and SN 6) compared to SN 2. While finer particles theoretically offer a larger surface area for bonding, the lower strength in SN 6 is attributed to particle agglomeration and saturation effects caused by the high surface energy of the fine dust, as hinted at the cohesive texture in the Dino-Lite observations (Figure **??**A). This supports the notion that without optimal dispersion, excessive particle refinement can lead to cluster formation, acting as stress concentrators rather than reinforcements [19]. Conversely, the coarser SN 2 particles facilitated better dispersion and promoted a rougher fracture surface via crack deflection mechanisms, effectively absorbing more energy during failure [20]. These findings confirm that PV waste can function as an effective reinforcement, provided that the particle size is optimized to

balance dispersion and interfacial bonding.

To clarify the strengthening mechanism observed in the flexural tests, the fracture surface morphologies were analyzed using SEM, as shown in Figure 7. The neat resin specimen (Figure 7A) displays a relatively smooth fracture surface with distinct riverlike patterns, corresponding to the lowest flexural strength of 19.13 MPa. This smooth topography indicates that crack propagation occurred with minimal resistance through the matrix.

In contrast, the composite specimens (Figure 7B-D) exhibit a transition toward rougher and more rugged fracture morphologies as the composite variation changes from SN 6 to SN 2. The presence of PV powder particles (indicated by arrows) disrupts the crack path. However, a distinct difference in filler dispersion is evident. In the SN 6 specimen (Figure 7B), the fine particles exhibit clear signs of agglomeration. As detailed in the magnified inset and quantitatively estimated using a 10 μm reference scale, a visible cluster measuring approximately 9-10 μm across can be observed, as indicated by the central arrows. (indicated by the central arrows). Morphologically, this cluster is not a single solid particle but rather a cohesive agglomerate composed of multiple finer submicron particles. Due to their small size and high surface energy, these fine particles have a strong tendency to cluster together rather than disperse uniformly within the resin matrix. This agglomeration has a detrimental effect on the composite's structural integrity because the inner core of these clusters often lacks proper resin infiltration (poor wetting), creating microscopic void-like pockets. Consequently, these localized agglomerates act as structural defects and stress concentrators under flexural loading. Microcracks can easily initiate and propagate at the weak interface between the agglomerates and the surrounding matrix, providing direct microstructural evidence for the premature failure and lower flexural strength (25.65 MPa) observed in the SN 6 composite.

As seen prominently in the SN 2 specimen (Figure 7D), the fracture surface is characterized by highly irregular, step-like structures. This phenomenon, known as crack deflection, forces cracks to travel along a more tortuous path around the rigid filler particles. Unlike the smooth fracture observed in the neat resin, these rigid inclusions act as physical obstacles that deflect the crack front, thereby increasing the total fracture surface area and the energy required for crack propagation. Furthermore, the mechanical enhancement is supported by micromechanical interlocking that occurs during the vat photopolymerization process. In this stage, the low-viscosity resin effectively penetrates the micro-topography and surface irregularities of the PV particles. Upon UV exposure within the DLP system, the resin solidifies around these features, creating a strong physical "grip" at the interface. This synergy between crack deflection and physical interlocking explains why the SN 2 variation, with its optimal particle distribution, achieved a 73% increase in ultimate

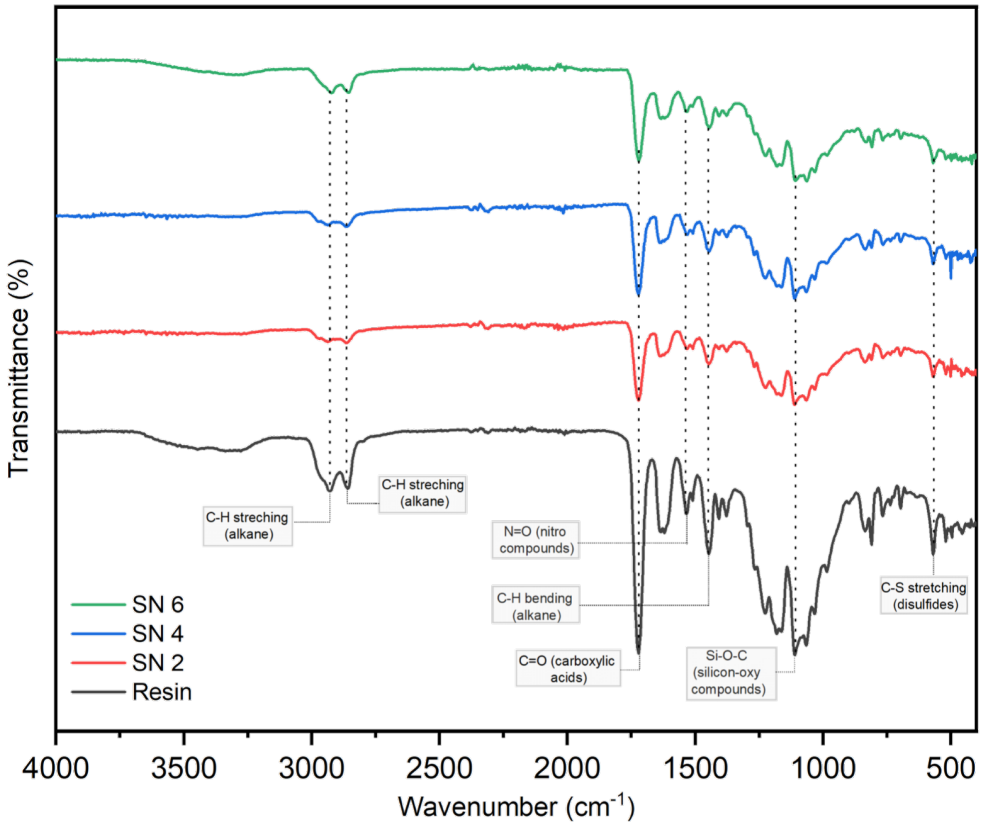

Figure 9. FTIR results of various specimens.

flexural strength to 33.11 MPa. This observation is consistent with the FTIR analysis (Section 3.4), which confirmed that the reinforcement mechanism is governed primarily by physical interfacial interactions rather than chemical cross-linking.

3.4. Chemical Composition

The Fourier Transform Infrared (FTIR) spectroscopy analysis, performed using a SHIMADZU IRTracer-100, elucidates the chemical interactions and functional group stability of the DLP-printed composites across the neat resin and the photovoltaic filler-loaded samples (SN 2, SN 4, and SN 6). The FTIR spectra are illustrated in Figure 9. The spectra exhibit characteristic absorption bands indicative of the polymer matrix, notably the prominent peaks at approximately 1720 cm^{-1} and 1100 cm^{-1}, which correspond to C=O (carboxylic acid) and Si−O−C (silicon-oxygen compounds) stretching vibrations, respectively. The presence of dual peaks between 2800 cm^{-1} and 3000 cm^{-1} represents C−H stretching of alkane groups, while additional bands corresponding to N=O (nitro compounds) and C−H bending vibrations are visible within the fingerprint region.

A comparative analysis of the four spectra shows that the primary functional groups of the resin remain chemically consistent even after the incorporation of the SN-series PV fillers. However, there is a noticeable reduction in the relative transmittance intensities as the filler particle size decreases from SN 2 to SN 6, particularly in the Si−O−C and C=O regions. This suggests that while the fillers are physically dispersed within the matrix without altering its fundamental chemical structure, the higher surface area of finer particles (SN 6) leads to more pronounced physical shielding or localized agglomeration. The detection of C−S stretching (disulfides) at the lower wavenumber region further characterizes the specific microstructural environment of the composite. In this context, this environment is defined by the close physical coexistence and mechanical contact between the resin matrix and the PV filler, rather than the formation of any new chemical bonds. This chemical stability confirms that the reinforcement mechanism is predominantly physical. Consequently, the enhanced flexural strength observed in the SN 2 variation is attributed to mechanical interlocking and crack deflection rather than chemical cross-linking. This preservation of key functional groups ensures the material's chemical integrity for sustainable applications [10].

4. Conclusions

This study demonstrates the viability of repurposing photovoltaic waste powder as a reinforcing filler in Digital Light Processing (DLP) 3D-printed resin composites. Morphological and elemental analysis (SEM-EDX) confirmed that the coarse, angular Silicon particles (SN 2) were effectively dispersed within the matrix, altering the fracture morphology from a smooth, brittle surface to a rugged, energy-absorbing texture driven by crack deflection mechanisms. FTIR spectroscopy further validated that the filler integration remained fundamentally physical, preserving the chemical stability of the resin without inducing degradation.

Mechanically, this physical interlocking resulted in a significant performance enhancement, with the SN 2 sample achieving a peak flexural strength of 33.11 MPa, a marked improvement over the 19.13 MPa baseline of the neat resin. Conversely, excessive particle refinement in the SN 6 variation led to agglomeration, likely due to the cohesive nature of the finer dust, which subsequently reduced the reinforcement efficiency. Ultimately, this research highlights that while PV waste is a sustainable reinforcement candidate, optimizing particle size to balance dispersion and interfacial bonding as successfully demonstrated by the SN 2 fraction, avoiding the pitfalls of ultra-fine powders is critical for maximizing the structural benefits in additive manufacturing applications.

Acknowledgments

The authors would like to express their gratitude to the CNC Laboratory at DTMI-FT Universitas Gadjah Mada for their invaluable contribution to this research by providing access to their facilities.

References

[1] C. C. Faircloth, K. H. Wagner, K. E. Woodward, P. Rakkwamsuk, and S. H. Gheewala, "The environmental and economic impacts of photovoltaic waste management in thailand," *Resources, Conservation and Recycling*, vol. 143, pp. 260–272, Apr. 2019.

[2] E. Klugmann-Radziemska, "Recycling of raw materials, silicon wafers and complete solar cells from photovoltaic modules," *Journal of Solar Energy Research Updates*, vol. 3, pp. 13–19, Sept. 2016.

[3] O. Khankhoje, H. Bherwani, and R. Biniwale, "Assessing life cycle environmental impacts of solar photovoltaics in india with a focus on end-of-life disposal," *Environmental Science and Pollution Research*, vol. 32, pp. 16098–16119, June 2025.

[4] P. Nain and A. Kumar, "Understanding metal dissolution from solar photovoltaics in msw leachate under standard waste characterization conditions for informing end-of-life photovoltaic waste management," *Waste Management*, vol. 123, pp. 97–110, Mar. 2021.

[5] G. Song, Y. Lu, B. Liu, H. Duan, H. Feng, and G. Liu, "Photovoltaic panel waste assessment and embodied material flows in china, 2000–2050," *Journal of Environmental Management*, vol. 338, p. 117675, July 2023.

[6] S. R. Kokul and S. Bhowmik, "Recycling of crystalline silicon photovoltaic solar panel waste to modified composite products," *Progress in Rubber, Plastics and Recycling Technology*, vol. 37, pp. 327–339, Nov. 2021.

[7] X. Tian, S. D. Stranks, and F. You, "Life cycle assessment of recycling strategies for perovskite photovoltaic modules," *Nature Sustainability*, vol. 4, pp. 821–829, Sept. 2021.

[8] C. He, Y. Zhuo, and Y. Shen, "Improving particle separation and recovery of valuable materials from end-of-life solar panels," *Resources, Conservation and Recycling*, vol. 225, p. 108594, Jan. 2026.

[9] H. Cao, N. Chen, S. Yang, X. Zhang, Q. Zou, and B. Wang, "An efficient separation method for a photovoltaic modules backsheet based on swelling and gas expansion at low temperature," *ACS Sustainable Chemistry & Engineering*, vol. 13, pp. 12782–12791, Aug. 2025.

[10] K. M. Nambiraj, K. Rajkumar, and P. Sabarinathan, "A novel approach on reusing silicon wafer kerf particle as potential filler material in polymer composite," *Silicon*, vol. 14, pp. 1537–1548, Feb. 2022.

[11] V. S. Efstratiadis, A. Argyros, P. Efthymiopoulos, G. Maliaris, N. K. Nasikas, and N. Michailidis, "Utilization of silica filler as reinforcement material of polylactic acid (pla) in 3d printing applications: Thermal, rheological, and mechanical performance," *Polymers*, vol. 16, p. 1326, May 2024.

[12] N. Mathur, S. Singh, and J. W. Sutherland, "Promoting a circular economy in the solar photovoltaic industry using life cycle symbiosis," *Resources, Conservation and Recycling*, vol. 155, p. 104649, Apr. 2020.

[13] E. Manoj, G. Selvakumar, V. Sivaprakash, and A. C, "Fabrication and characterization of porous biochar and si3n4 bioceramic toughened natural fibre epoxy composite," *Silicon*, vol. 17, pp. 2417–2428, July 2025.

[14] N. Lakshmaiya, S. R. Kota, K. Bhaskar, A. Palanivel, N. D. K. R. Chukka, and R. Maranan, "Sustainable hybrid epoxy composites reinforced with kenaf fiber banana peel waste and sic for multifunctional performance," *Results in Engineering*, vol. 28, p. 107558, Dec. 2025.

[15] S. Siraj, A. H. Al-Marzouqi, M. Z. Iqbal, and W. Ahmed, "Impact of micro silica filler particle size on mechanical properties of polymeric based composite material," *Polymers*, vol. 14, Nov. 2022.

[16] E. Supriyanto, N. K. Yudha, A. D. Nugroho, and M. A. Muflikhun, "Characteristics and evaluation of recycled waste pvcs as a filler in composite structures: Validation through simulation and experimental methods," *Composites Part C: Open Access*, vol. 15, p. 100525, Oct. 2024.

[17] ASTM International, "ASTM D790-15: Standard Test Methods for Flexural Properties of Unreinforced and Reinforced Plastics and Electrical Insulating Materials," 2015. Accessed: 2026-02-14.

[18] J. Coates, "Interpretation of infrared spectra, a practical approach," in *Encyclopedia of Analytical Chemistry* (R. A. Meyers, ed.), Wiley, 2000.

[19] A.-M. Kayaba, O. Issakah, S. Akromah, E. E. Nettey-Oppong, and E. K. A. Asare, "Synergistic effects of micro- and macro-sized palm kernel shell fillers on the tensile properties of hdpe composites," *Royal Society Open Science*, vol. 12, p. 241911, July 2025.

[20] S. Samal, "Effect of shape and size of filler particle on the aggregation and sedimentation behavior of the polymer composite," *Powder Technology*, vol. 366, pp. 43–51, Apr. 2020.